

Imaging and dynamics for physical and life sciences

Resolving the Effect of Oxygen Vacancies on Co Nanostructures Using Soft XAS/X-PEEM

A.M. Beale, C. Qiu, Y. Odarchenko, I. Lezcano-Gonzalez (Department of Chemistry, University College London, UK; Research Complex at Harwell, Rutherford Appleton Laboratory, Harwell, Didcot, UK)
Q. Meng (School of Chemical Engineering and Light Industry, Guangdong University of Technology, Guangzhou, China)

S. Xu (Research Complex at Harwell, Rutherford Appleton Laboratory, Harwell, Didcot, UK; Cardiff Catalysis Institute, School of Chemistry, Cardiff University, UK)
P. Olalde-Velasco, F. Maccherozzi (Diamond Light Source, Harwell Science and Innovation Campus, Didcot, UK)
L. Zanetti-Domingues, M. Martin-Fernandez (Central Laser Facility, Research Complex at Harwell, STFC Rutherford Appleton Laboratory, Harwell Campus, Didcot, UK)

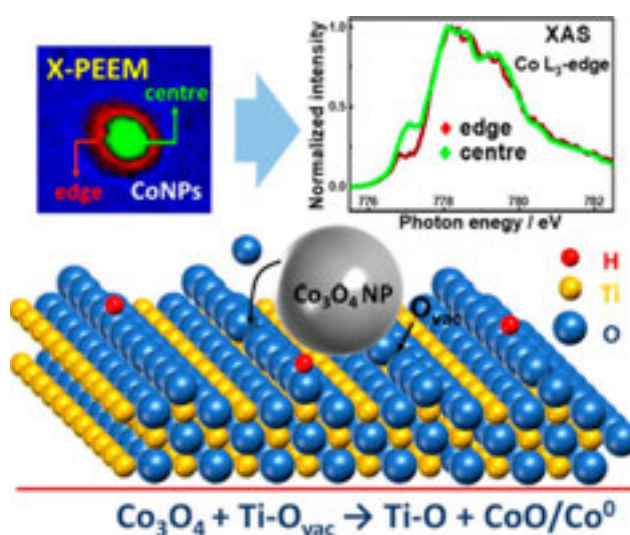
Improving both the extent of metallic Co nanoparticle (Co NP) formation and their stability is necessary to ensure good catalytic performance, particularly for Fischer-Tropsch synthesis (FTS). Here, we observe how the presence of surface oxygen vacancies (O_{vac}) on TiO_2 can readily reduce individual Co_3O_4 NPs directly into CoO/Co^0 in the freshly prepared sample by using a combination of X-ray photoemission electron microscopy (X-PEEM) coupled with soft X-ray absorption spectroscopy. The O_{vac} are particularly good at reducing the edge of the NPs as opposed to their centre, leading to smaller particles being more reduced than larger ones.

We then show how further reduction (and O_{vac} consumption) is achieved during heating in H_2 /syngas ($H_2 + CO$) and reveal that O_{vac} also prevents total reoxidation of Co NPs in syngas, particularly the smallest (~ 8 nm) particles, thus maintaining the presence of metallic Co, potentially improving catalyst performance.

Reproduced from ACS Catal. 2022, 12, 9125–9134, published by American Chemical Society, under the terms of a Creative Commons Attribution (CC BY) license (<http://creativecommons.org/licenses/by/4.0/>) doi: 10.1021/acscatal.2c00611

Contact:

A.M. Beale
andrew.beale@ucl.ac.uk



Multi-dimensional and spatiotemporal correlative imaging at the plasma membrane of live cells to determine the continuum nano-to-micro scale lipid adaptation and collective motion

M. Bernabé-Rubio (Department of Cell Biology and Immunology, Centro de Biología Molecular Severo Ochoa, Consejo Superior de Investigaciones Científicas and Universidad Autónoma de Madrid, Spain; King's College London Centre for Stem Cells and Regenerative Medicine, Guy's Campus, London, UK)

M. Bosch-Fortea (Department of Cell Biology and Immunology, Centro de Biología Molecular Severo Ochoa, Consejo Superior de Investigaciones Científicas and Universidad Autónoma de Madrid, Spain; Institute of Bioengineering and School of Engineering and Materials Science, Queen Mary, University of London, UK)

M.A. Alonso (Department of Cell Biology and Immunology, Centro de Biología Molecular Severo Ochoa, Consejo Superior de Investigaciones Científicas and Universidad Autónoma de Madrid, Spain)

J. Bernardino de la Serna (Central Laser Facility, Research Complex at Harwell, STFC Rutherford Appleton Laboratory, Harwell Campus, Didcot, UK; National Heart and Lung Institute, Imperial College London, UK; NIHR Imperial Biomedical Research Centre, London, UK)

The primary cilium is a specialized plasma membrane protrusion with important receptors for signalling pathways. In polarized epithelial cells, the primary cilium assembles after the midbody remnant (MBR) encounters the centrosome at the apical surface. The membrane surrounding the MBR, namely remnant-associated membrane patch (RAMP), once situated next to the centrosome, releases some of its lipid components to form a centrosome-associated membrane patch (CAMP) from which the ciliary membrane stems.

The RAMP undergoes a spatiotemporal membrane refinement during the formation of the CAMP, which becomes highly enriched in condensed membranes with low lateral mobility. To better understand this process, we have developed a correlative imaging approach that yields quantitative information about the lipid lateral packing, its mobility and collective assembly at the plasma membrane at different spatial scales over time. Our work paves the way towards a quantitative understanding of the spatiotemporal lipid collective assembly at the plasma membrane as a functional determinant in cell biology and its direct correlation with the membrane physicochemical state.

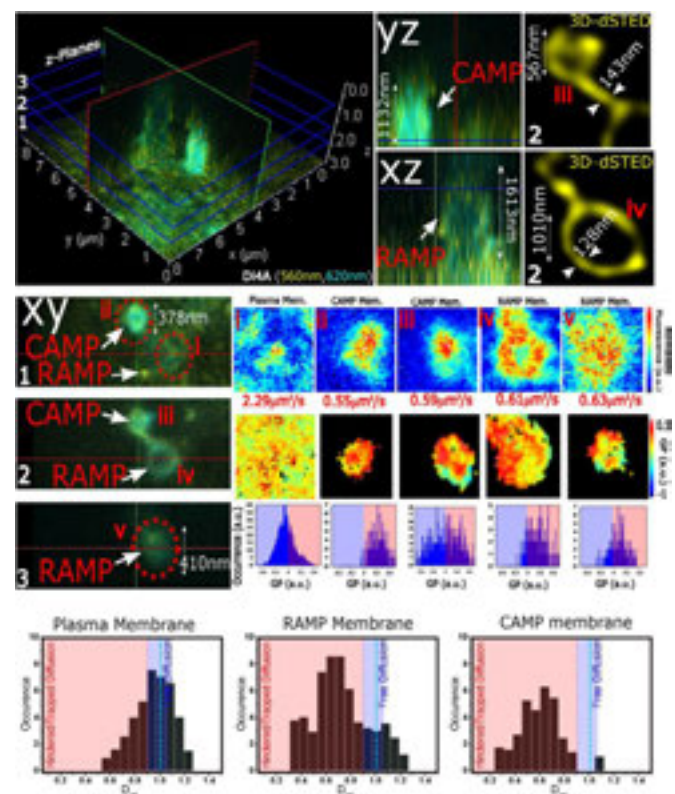
These findings allowed us to gain a deeper insight into the mechanisms behind the biogenesis of the ciliary membrane of polarized epithelial cells.

Reproduced from the bioRxiv preprint version (which was not certified by peer review), doi: <https://doi.org/10.1101/2021.03.02.433589>; this version posted March 2, 2021. It is made available under a [CC-BY-NC-ND 4.0 International license](https://creativecommons.org/licenses/by-nc-nd/4.0/). A definitive version was subsequently published in *Methods*, Volume 193, September 2021, Pages 136-147 © Elsevier 2021 doi: 10.1016/j.jymeth.2021.06.007

Contact:

J. Bernardino de la Serna

j.bernardino-de-la-serna@imperial.ac.uk



The RAMP has domains with condensed membrane and slow-moving constituents

MDCK cells showing a RAMP/CAMP labelled with Di4A. Top row panel, to the left-hand-side: large orthogonal axial reconstruction of raw micrograph view showing below at the central panel (left-hand-side) the XY section at 3 z-planes (z1: proximal, z2: middle and z3: distal); central images: YZ and XZ projections; right-hand-side images: zoomed-in deconvolved super-resolution STED image of the z2 middle plane. Central row panel to the right-hand-side from top to bottom row: diffusion coefficient values, intensity map and GP map of each of the cross sections z1-z3 and a plasma membrane region and occurrence histograms of GP values for cross sections z1- z3 and a plasma membrane region. Bottom row panel: frequency histograms obtained from LICSR showing the Drat at the plasma membrane, RAMP and CAMP (>15 regions of interest from >7 cells). Red-shadowed region indicates hindered or trapped diffusion; blue-shadowed region indicates free diffusion.

Real-time imaging and analysis of cell-hydrogel interplay within an extrusion-bioprinting capillary

G. Poologasundarampillai, S. Nagi Jayash (School of Dentistry, Institute of Clinical Sciences, University of Birmingham, UK)
A. Haweet (School of Dentistry, Institute of Clinical Sciences, University of Birmingham, UK; Central Laser Facility, Research Complex at Harwell, STFC Rutherford Appleton Laboratory, Harwell Campus, Didcot, UK)

G. Morgan, J.E. Moore Jr (Department of Bioengineering, Imperial College London)
A. Candeo (Central Laser Facility, Research Complex at Harwell, STFC Rutherford Appleton Laboratory, Harwell Campus, Didcot, UK; Dipartimento di Fisica, Politecnico di Milano, Italy)

Additive manufacturing platforms are transforming research and industrial sectors worldwide. In regenerative medicine and pharmaceutical applications, they facilitate the development of patient-specific devices for implantation, as well as in vitro models of tissues and organs for disease modelling and drug screening. A key example is extrusion-based bioprinting, where a bioink that contains cells, biomolecules and a support matrix (often hydrogel), is extruded through a narrow capillary onto a platform forming the desired structure. The printing parameters and hydrogel flow behavior likely determine the extent to which cells are damaged mechanically as they pass through the capillary. Here, we present direct observations of the hydrogels and suspended cells during the printing process to help elucidate conditions potentially leading to mechanical damage and cell death. Light-sheet fluorescence microscopy was applied to observe the real-time flow of bioinks through a capillary mimicking the conditions found in bioprinting.

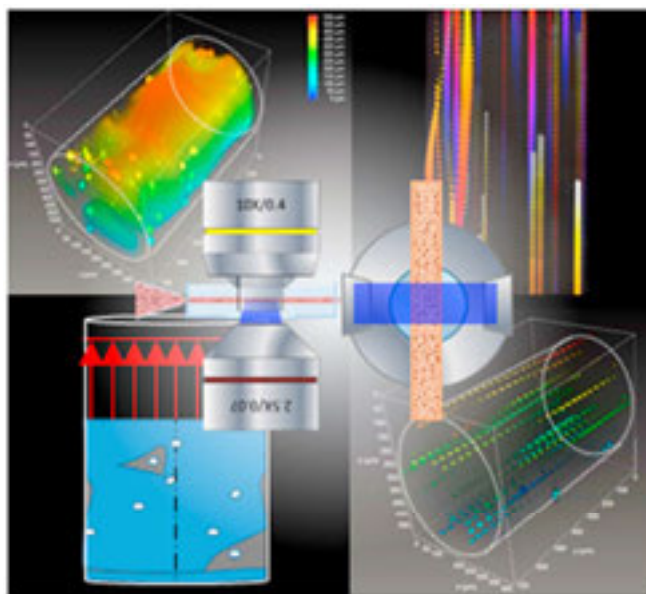
Bioink formulations exhibiting constant and shear thinning viscosities, along with UV-crosslinked gelatin methacryl (GelMA) were studied, and cell viability of post-printed gels were measured via fluorescent imaging. Cell tracking enabled flow profiles of bioinks to be deduced. In agreement with current flow simulations, the constant and shear thinning formulations displayed a Poiseuille flow profile although with a plug velocity profile for the latter.

The UV-crosslinked GelMA formulation exhibited a two-phase annular flow with gel morphologies depicting gross-melt fractures attributed to over-gelled hydrogels. Cell viability was higher in UV-crosslinked GelMA at high flow rates compared to uncrosslinked GelMA. The findings presented here will improve modeling cell-material flow during bioprinting through accurate estimation of flow conditions, in particular for complex materials. The novel imaging approach could be further exploited to provide process monitoring and feedback to improve the outcomes of 3D bioprinting.

Reproduced from G Poologasundarampillai et al 2021 *Bioprinting* **23** e00144, under the terms of a Creative Commons Attribution (CC BY) license (<http://creativecommons.org/licenses/by/4.0/>). doi: 10.1016/j.bprint.2021.e00144

Contact:

A. Candeo
alessia.candeo@polimi.it



Super-Resolution Microscopy Using a Bioorthogonal-Based Cholesterol Probe Provides Unprecedented Capabilities for Imaging Nanoscale Lipid Heterogeneity in Living Cells

M. Lorizate, M. Calleja-Felipe (Department of Biochemistry and Molecular Biology, University of the Basque Country (UPV/EHU) and Instituto Biofisika (UPV/EHU, CSIC), Spain)

F-X. Contreras (Department of Biochemistry and Molecular Biology, University of the Basque Country (UPV/EHU) and Instituto Biofisika (UPV/EHU, CSIC), Spain; IKERBASQUE, Basque Foundation for Science, Bilbao, Spain)

O. Terrones, J. Olazar-Intxausti (Department of Biochemistry and Molecular Biology, University of the Basque Country (UPV/EHU), Spain)

J.A. Nieto-Garai, I. Rojo-Bartolomé, O. Morana, A. Arboleaya (Department of Biochemistry and Molecular Biology, University of the Basque Country (UPV/EHU) and Instituto Biofisika (UPV/EHU, CSIC), Spain; Fundación Biofísica Bizkaia/Biofísica Bizkaia Fundazioa (FBB), Spain)

D. Ciceri (Fundación Biofísica Bizkaia/Biofísica Bizkaia Fundazioa (FBB), Spain)

A. Martin (National Heart and Lung Institute, Imperial College London, UK)

M. Szykiewicz (Central Laser Facility, Research Complex at Harwell, STFC Rutherford Appleton Laboratory, Harwell Campus, Didcot, UK)

J. Bernardino de la Serna (National Heart and Lung Institute, Imperial College London, UK; Central Laser Facility, Research Complex at Harwell, STFC Rutherford Appleton Laboratory, Harwell Campus, Didcot, UK; NIHR Imperial Biomedical Research Centre, London, UK)

Despite more than 20 years of work since the lipid raft concept was proposed, the existence of these nanostructures remains highly controversial due to the lack of noninvasive methods to investigate their native nanorganization in living unperturbed cells. There is an unmet need for probes for direct imaging of nanoscale membrane dynamics with high spatial and temporal resolution in living cells. In this paper, a bioorthogonal-based cholesterol probe (chol- N_3) is developed that, combined with nanoscopy, becomes a new powerful method for direct visualization and characterization of lipid raft at unprecedented resolution in living cells.

The chol- N_3 probe mimics cholesterol in synthetic and cellular membranes without perturbation. When combined with live-cell super-resolution microscopy, chol- N_3 demonstrates the existence of cholesterol-rich nanodomains of <50 nm at the plasma membrane of resting living cells. Using this tool, the lipid membrane structure of such subdiffraction limit domains is identified, and the nanoscale spatiotemporal organization of cholesterol in the plasma membrane of living cells reveals multiple cholesterol diffusion modes at different spatial localizations. Finally, imaging across thick organ samples outlines the potential of this new method to address essential biological questions that were previously beyond reach.

Reproduced from Lorizate, Maier et al. "Super-Resolution Microscopy Using a Bioorthogonal-Based Cholesterol Probe Provides Unprecedented Capabilities for Imaging Nanoscale Lipid Heterogeneity in Living Cells." *Small methods* vol. 5,9 (2021): e2100430, under of a Creative Commons Attribution (CC BY) license (<http://creativecommons.org/licenses/by/4.0/>). doi:10.1002/smt.202100430

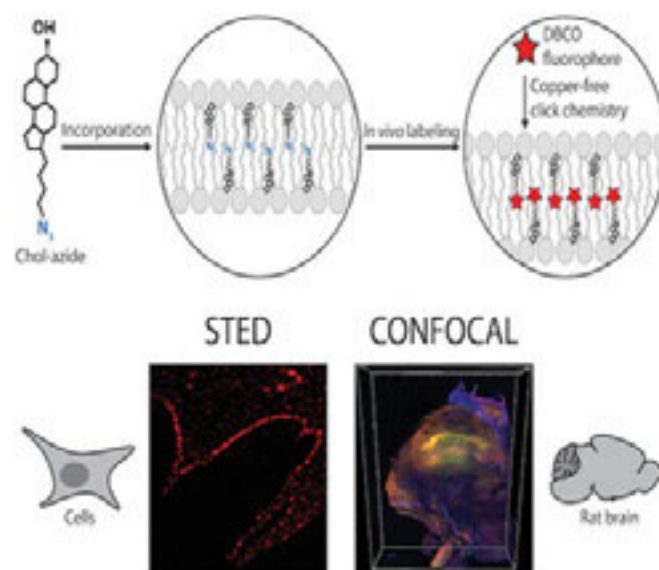
Contact:

F-X. Contreras

xabier.contreras@ehu.eus

J. Bernardino de la Serna

j.bernardino-de-la-serna@imperial.ac.uk



Direct imaging and characterization of nanoscale lipid heterogeneity in living cells with high temporal and spatial resolution using developed bioorthogonal cholesterol probe and nanoscopy are introduced. This probe enables tackling biological questions that were previously beyond reach. Visualization of cholesterol distribution through thick tissues outlines the tool's potential to investigate the role of cholesterol in health and disease.

Identification of a New Cholesterol-Binding Site within the IFN- γ Receptor that is Required for Signal Transduction

O. Morana, J.A. Nieto-Garai, A. Arboleya, D. Ciceri, I. Rojo-Bartolomé (Instituto Biofisika (UPV/EHU, CSIC), University of the Basque Country (UPV/EHU), Spain; Fundació Biofisika Bizkaia/Biofisika Bizkaia Fundazioa (FBB), University of the Basque Country (UPV/EHU), Spain; Department of Biochemistry and Molecular Biology, Faculty of Science and Technology, University of the Basque Country (UPV/EHU), Spain)

P. Björkholm (Center for Biomembrane Research, Department of Biochemistry and Biophysics, Stockholm University, Sweden; Science for Life Laboratory, Stockholm University, Sweden)

O. Terrones (Department of Biochemistry and Molecular Biology, Faculty of Science and Technology, University of the Basque Country (UPV/EHU), Spain)

C.M. Blouin, C. Lamaze (Institut Curie - Centre de Recherche, PSL Research University, Membrane Mechanics and Dynamics of Intracellular Signaling Laboratory, Paris, France; Institut National de la Santé et de la Recherche Médicale (INSERM), Paris, France; Centre National de la Recherche Scientifique (CNRS), Paris, France)

M. Lorizate (Instituto Biofisika (UPV/EHU, CSIC), University of the Basque Country (UPV/EHU), Spain; Department of Biochemistry and Molecular Biology, Faculty of Science and Technology, University of the Basque Country (UPV/EHU), Spain)

F.-X. Contreras (Instituto Biofisika (UPV/EHU, CSIC), University of the Basque Country (UPV/EHU), Spain; Department of Biochemistry and Molecular Biology, Faculty of Science and Technology, University of the Basque Country (UPV/EHU), Spain; IKERBASQUE, Basque Foundation for Science, Bilbao, Spain)

J. Bernardino de la Serna (National Heart and Lung Institute, Imperial College London, UK; Central Laser Facility, Research Complex at Harwell, STFC Rutherford Appleton Laboratory, Harwell Campus, Didcot, UK; NIHR Imperial Biomedical Research Centre, London, UK)

The cytokine interferon-gamma (IFN- γ) is a master regulator of innate and adaptive immunity involved in a broad array of human diseases that range from atherosclerosis to cancer. IFN- γ exerts its signalling action by binding to a specific cell surface receptor, the IFN- γ receptor (IFN- γ R), whose activation critically depends on its partition into lipid nanodomains. However, little is known about the impact of specific lipids on IFN- γ R signal transduction activity. Here, a new conserved cholesterol (chol) binding motif localized within its single transmembrane domain is identified.

Through direct binding, chol drives the partition of IFN- γ R2 chains into plasma membrane lipid nanodomains, orchestrating IFN- γ R oligomerization and transmembrane signalling. Bioinformatics studies show that the signature sequence stands for a conserved chol-binding motif presented in many mammalian membrane proteins.

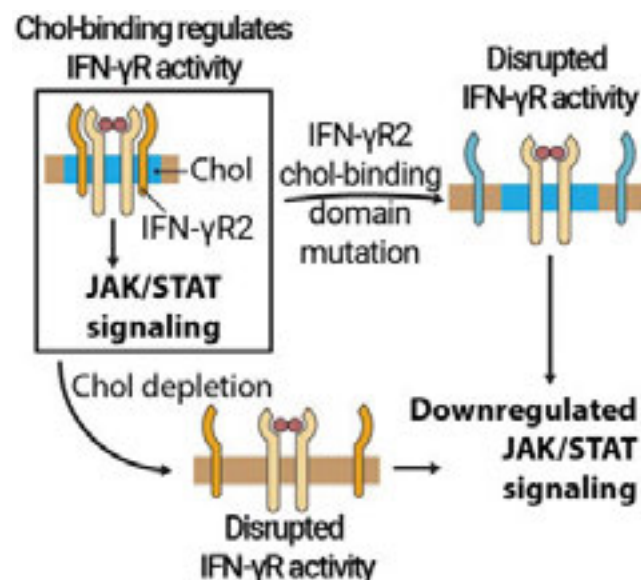
The discovery of chol as the molecular switch governing IFN- γ R transmembrane signalling represents a significant advance for understanding the mechanism of lipid selectivity by membrane proteins, but also for figuring out the role of lipids in modulating cell surface receptor function. Finally, this study suggests that inhibition of the chol-IFN γ R2 interaction may represent a potential therapeutic strategy for various IFN- γ -dependent diseases.

Reproduced from Morana, O. et al. *Adv. Sci.* 2022, **9**, 2105170, published by Wiley-VCH GmbH, under the terms of a Creative Commons Attribution (CC BY) license (<http://creativecommons.org/licenses/by/4.0/>) doi: 10.1002/adv.202105170

Contact:

F.-X. Contreras

xabier.contreras@ehu.eus



This work uncovers the role of cholesterol as the molecular determinant controlling interferon-gamma receptor (IFN- γ R) activity. Through a multidisciplinary approach the structural signature within the IFN- γ R required for cholesterol binding is identified. Binding of cholesterol is critical for receptor plasma membrane compartmentalization, heterodimerization, and signal transduction. This work identifies a therapeutic target for prevention and treatment of IFN- γ dependent diseases.

Measurement of gas-phase OH radical oxidation and film thickness of organic films at the air–water interface using material extracted from urban, remote and wood smoke aerosol

R.H. Shepherd (Central Laser Facility, Research Complex at Harwell, STFC Rutherford Appleton Laboratory, Harwell Campus, Didcot, UK; Department of Earth Sciences, Royal Holloway, University of London, UK)

M.D. King (Department of Earth Sciences, Royal Holloway, University of London, UK)

A.R. Rennie (Department of Chemistry – Ångström Laboratory, Uppsala University, Sweden)

A.D. Ward (Central Laser Facility, Research Complex at Harwell, STFC Rutherford Appleton Laboratory, Harwell Campus, Didcot, UK)

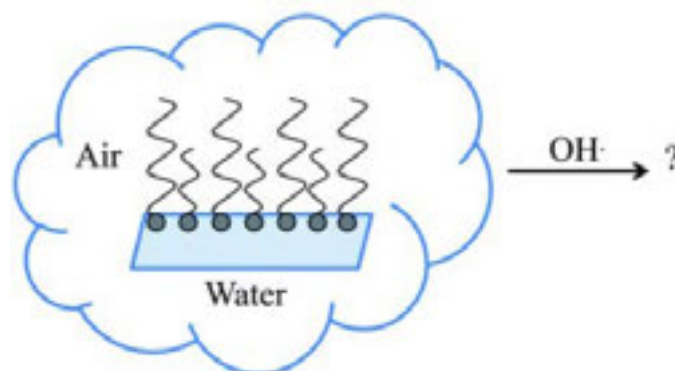
M.M. Frey, N. Brough, J. Eveson, S. Del Vento (British Antarctic Survey, Natural Environment Research Council, Cambridge, UK)

A. Milsom, C. Pfrang (School of Geography, Earth and Environmental Sciences, University of Birmingham, UK)

M.W.A. Skoda, R.J.L. Welbourn (ISIS Pulsed Neutron and Muon Source, STFC Rutherford Appleton Laboratory, Harwell Campus, Didcot, UK)

The presence of an organic film on a cloud droplet or aqueous aerosol particle has the potential to alter the chemical, optical and physical properties of the droplet or particle. In the study presented, water insoluble organic materials extracted from urban, remote (Antarctica) and wood burning atmospheric aerosol were found to have stable, compressible, films at the air–water interface that were typically $\sim 6\text{--}18$ Å thick. These films are reactive towards gas-phase OH radicals and decay exponentially, with bimolecular rate constants for reaction with gas-phase OH radicals of typically $0.08\text{--}1.5 \times 10^{-10} \text{ cm}^3 \text{ molecule}^{-1} \text{ s}^{-1}$. These bimolecular rate constants equate to initial OH radical uptake coefficients estimated to be $\sim 0.6\text{--}1$ except woodsmoke (~ 0.05).

The film thickness and the neutron scattering length density of the extracted atmosphere aerosol material (from urban, remote and wood burning) were measured by neutron reflection as they were exposed to OH radicals. For the first time neutron reflection has been demonstrated as an excellent technique for studying the thin films formed at air–water interfaces from materials extracted from atmospheric aerosol samples.



Additionally, the kinetics of gas-phase OH radicals with a proxy compound, the lipid 1,2-distearoyl-*sn*-glycero-3-phosphocholine (DSPC) was studied displaying significantly different behaviour, thus demonstrating it is not a good proxy for atmospheric materials that may form films at the air–water interface. The atmospheric lifetimes, with respect to OH radical oxidation, of the insoluble organic materials extracted from atmospheric aerosol at the air–water interface were a few hours. Relative to a possible physical atmospheric lifetime of 4 days, the oxidation of these films is important and needs inclusion in atmospheric models. The optical properties of these films were previously reported [Shepherd *et al.*, *Atmos. Chem. Phys.*, 2018, **18**, 5235–5252] and there is a significant change in top of the atmosphere albedo for these thin films on core–shell atmospheric aerosol using the film thickness data and confirmation of stable film formation at the air–water interface presented here.

Reproduced from *Environ. Sci.: Atmos.*, 2022, **2**, 574, published by the Royal Society of Chemistry, under the terms of a Creative Commons Attribution (CC BY) license (<http://creativecommons.org/licenses/by/3.0/>). doi: 10.1039/D2EA00013J

Contact:

M.D. King

m.king@rhul.ac.uk

Mie scattering from optically levitated mixed sulfuric acid–silica core–shell aerosols: observation of core–shell morphology for atmospheric science

M.R. McGrory, R.H. Shepherd (Central Laser Facility, Research Complex at Harwell, STFC Rutherford Appleton Laboratory, Harwell Campus, Didcot, UK; Department of Earth Sciences, Royal Holloway, University of London, UK)

M.D. King (Department of Earth Sciences, Royal Holloway, University of London, UK)

N. Davidson, F.D. Pope (School of Geography, Earth and Environmental Sciences, University of Birmingham, UK)

I.M. Watson (School of Earth Science, University of Bristol, UK)

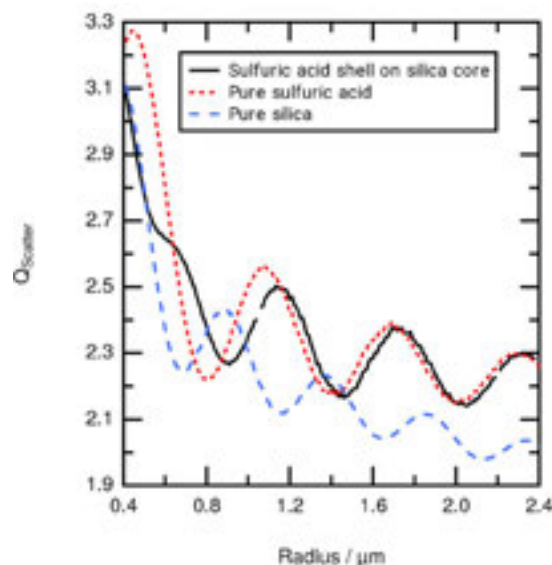
R.G. Grainger (National Centre for Earth Observation, Atmospheric, Oceanic and Planetary Physics, University of Oxford, UK)

A.C. Jones (Met Office, Exeter, UK; College of Engineering Maths and Physical Sciences, University of Exeter, UK)

A.D. Ward (Central Laser Facility, Research Complex at Harwell, STFC Rutherford Appleton Laboratory, Harwell Campus, Didcot, UK)

Sulfuric acid is shown to form a core–shell particle on a micron-sized, optically-trapped spherical silica bead. The refractive indices of the silica and sulfuric acid, along with the shell thickness and bead radius were determined by reproducing Mie scattered optical white light as a function of wavelength in Mie spectroscopy. Micron-sized silica aerosols (silica beads were used as a proxy for atmospheric silica minerals) were levitated in a mist of sulfuric acid particles; continuous collection of Mie spectra throughout the collision of sulfuric acid aerosols with the optically trapped silica aerosol demonstrated that the resulting aerosol particle had a core–shell morphology.

Contrastingly, the collision of aqueous sulfuric acid aerosols with optically trapped polystyrene aerosol resulted in a partially coated system. The light scattering from the optically levitated aerosols was successfully modelled to determine the diameter of the core aerosol ($\pm 0.003 \mu\text{m}$), the shell thickness ($\pm 0.0003 \mu\text{m}$) and the refractive index (± 0.007). The experiment demonstrated that the presence of a thin film rapidly changed the light scattering of the original aerosol.



When a $1.964 \mu\text{m}$ diameter silica aerosol was covered with a film of sulfuric acid $0.287 \mu\text{m}$ thick, the wavelength dependent Mie peak positions resembled sulfuric acid. Thus mineral aerosol advected into the stratosphere would likely be coated with sulfuric acid, with a core–shell morphology, and its light scattering properties would be effectively indistinguishable from a homogenous sulfuric acid aerosol if the film thickness was greater than a few 100s of nm for UV-visible wavelengths.

Reproduced from *Phys. Chem. Chem. Phys.*, 2022, **24**, 5813, published by the Royal Society of Chemistry, under the terms of a Creative Commons Attribution (CC BY) license (<http://creativecommons.org/licenses/by/3.0/>). doi: 10.1039/d1cp04068e

Contact:

A.D. Ward

andy.ward@stfc.ac.uk

A Dinuclear Osmium(II) Complex Near-Infrared Nanoscopy Probe for Nuclear DNA

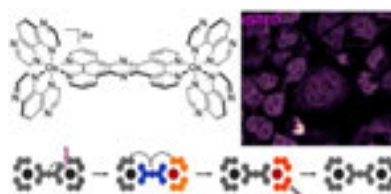
A.J.H.M. Meijer, J.A. Thomas, S.A. Archer, C.C. Robertson, S. Sreedharan, H. Carson (Department of Chemistry, University of Sheffield, UK)
B. Dietzek-Ivanšić, F. Dröge (Institute of Physical Chemistry, Friedrich Schiller University Jena, Germany; Leibniz Institute for Photonic Technology Jena e.V., Germany)
F.F. Noakes (Department of Chemistry and Department of Biomedical Science, University of Sheffield, UK)

A. Raza, S. MacNeil, J.W. Haycock (Materials Science & Engineering, University of Sheffield, UK)
C.G.W. Smythe (Department of Biomedical Science, University of Sheffield, UK)
J. Bernardino de la Serna (Central Laser Facility, Research Complex at Harwell, STFC Rutherford Appleton Laboratory, Harwell Campus, Didcot, UK; National Heart and Lung Institute, Faculty of Medicine, Imperial College London, UK)

With the aim of developing photostable nearinfrared cell imaging probes, a convenient route to the synthesis of heteroleptic Os^{II} complexes containing the Os(TAP)₂ fragment is reported. This method was used to synthesize the dinuclear Os^{II} complex, [(Os(TAP)₂)₂tpphz]⁴⁺ (where tpphz = tetrapyrido[3,2-a:2',3'-c:3'',2''-h:2''',3''''-j]phenazine and TAP = 1,4,5,8-tetraazaphenanthrene). Using a combination of resonance Raman and time-resolved absorption spectroscopy, as well as computational studies, the excited state dynamics of the new complex were dissected. These studies revealed that, although the complex has several close lying excited states, its near-infrared, NIR, emission ($\lambda_{\text{max}} = 780 \text{ nm}$) is due to a low-lying Os \rightarrow TAP based ³MCLT state. Cell-based studies revealed that unlike its Ru^{II} analogue, the new complex is neither cytotoxic nor photocytotoxic. However, as it is highly photostable as well as live-cell permeant and displays NIR luminescence within the biological optical

window, its properties make it an ideal probe for optical microscopy, demonstrated by its use as a super-resolution NIR STED probe for nuclear DNA.

Reproduced with permission from *J. Am. Chem. Soc.* 2021, 143, 48, 20442–20453, © 2021 American Chemical Society. doi: 10.1021/jacs.1c10325



Contact:

A.J.H.M. Meijer
a.meijer@sheffield.ac.uk

B. Dietzek-Ivanšić
benjamin.dietzek@uni-jena.de

J.A. Thomas
james.thomas@sheffield.ac.uk

The impact of molecular self-organisation on the atmospheric fate of a cooking aerosol proxy

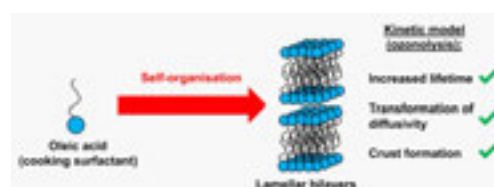
A. Milsom (School of Geography, Earth and Environmental Sciences, University of Birmingham, UK)
A.M. Squires (Department of Chemistry, University of Bath, UK)

A.D. Ward (Central Laser Facility, Research Complex at Harwell, STFC Rutherford Appleton Laboratory, Harwell Campus, Didcot, UK)
C. Pfrang (School of Geography, Earth and Environmental Sciences, University of Birmingham, UK; Department of Meteorology, University of Reading, UK)

Atmospheric aerosols influence the climate via cloud droplet nucleation and can facilitate the long-range transport of harmful pollutants. The lifetime of such aerosols can therefore determine their environmental impact. Fatty acids are found in organic aerosol emissions with oleic acid, an unsaturated fatty acid, being a large contributor to cooking emissions. As a surfactant, oleic acid can self-organise into nanostructured lamellar bilayers with its sodium salt, and this self-organisation can influence reaction kinetics. We developed a kinetic multi-layer model-based description of decay data we obtained from laboratory experiments of the ozonolysis of coated films of this self-organised system, demonstrating a decreased diffusivity for both oleic acid and ozone due to lamellar bilayer formation. Diffusivity was further inhibited by a viscous oligomer product forming in the surface layers of the film. Our results indicate that nanostructure formation can increase the reactive half-life of oleic acid by an order of

days at typical indoor and outdoor atmospheric ozone concentrations. We are now able to place nanostructure formation in an atmospherically meaningful and quantifiable context. These results have implications for the transport of harmful pollutants and the climate.

Reproduced from Milsom, A., Squires, A. M., Ward, A. D., and Pfrang, C.: The impact of molecular self-organisation on the atmospheric fate of a cooking aerosol proxy, *Atmos. Chem. Phys.*, **22**, 4895–4907, 2022, under the terms of a Creative Commons Attribution (CC BY) license (<http://creativecommons.org/licenses/by/4.0/>) doi:10.5194/acp-22-4895-2022



Contact:

C. Pfrang
c.pfrang@bham.ac.uk

Sphingomyelin Depletion Inhibits CXCR4 Dynamics and CXCL12-Mediated Directed Cell Migration in Human T Cells

S.R. Gardeta, E.M. García-Cuesta, G. D'Agostino, B. Soler Palacios, A. Quijada-Freire, P. Lucas, J.M. Rodríguez-Frade, M. Mellado (Chemokine Signaling Group, Department of Immunology and Oncology, National Center for Biotechnology/Consejo Superior de Investigaciones Científicas, Madrid, Spain)

J. Bernardino de la Serna (National Heart and Lung Institute, Imperial College London, UK; Central Laser Facility, Research Complex at Harwell, STFC Rutherford Appleton Laboratory, Harwell Campus, Didcot, UK; NIHR Imperial Biomedical Research Centre, London, UK)

C. Gonzalez-Riano, C. Barbas (Metabolomic and Bioanalysis Center (CEMBIO), Pharmacy Faculty, Centro de Estudios Universitarios, Madrid, Spain)

Sphingolipids, ceramides and cholesterol are integral components of cellular membranes, and they also play important roles in signal transduction by regulating the dynamics of membrane receptors through their effects on membrane fluidity. Here, we combined biochemical and functional assays with single-particle tracking analysis of diffusion in the plasma membrane to demonstrate that the local lipid environment regulates CXCR4 organization and function and modulates chemokine-triggered directed cell migration.

Prolonged treatment of T cells with bacterial sphingomyelinase promoted the complete and sustained breakdown of sphingomyelins and the accumulation of the corresponding ceramides, which altered both membrane fluidity and CXCR4 nanoclustering and dynamics.

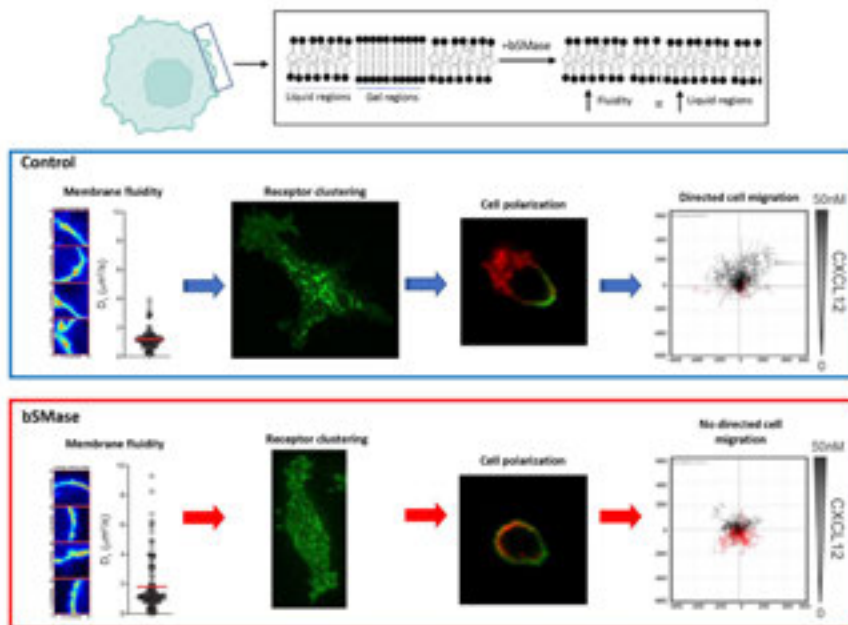
Under these conditions CXCR4 retained some CXCL12-mediated signaling activity but failed to promote efficient directed cell migration. Our data underscore a critical role for the local lipid composition at the cell membrane in regulating the lateral mobility of chemokine receptors, and their ability to dynamically increase receptor density at the leading edge to promote efficient cell migration.

Palacios B, Quijada-Freire A, Lucas P, Bernardino de la Serna J, Gonzalez-Riano C, Barbas C, Rodríguez-Frade JM and Mellado M (2022) Sphingomyelin Depletion Inhibits CXCR4 Dynamics and CXCL12-Mediated Directed Cell Migration in Human T Cells. *Front. Immunol.* **13**:925559, under the terms of a Creative Commons Attribution (CC BY) license (<http://creativecommons.org/licenses/by/4.0/>) doi: 10.3389/fimmu.2022.925559

Contact:

M. Mellado

mmellado@cnb.csic.es



By increasing membrane fluidity, bSMase treatment alters receptor clustering, cell polarization and the ability of cells to sense chemotactic gradients.

AR cooperates with SMAD4 to maintain skeletal muscle homeostasis

M. Forouhan, W.F. Lim, T.C. Roberts, A.A. Speciale, R. Ellerington, A. Garcia-Guerra (Department of Paediatrics, University of Oxford, UK)
L.C. Zanetti-Domingues, C.J. Tynan (Central Laser Facility, Research Complex at Harwell, STFC Rutherford Appleton Laboratory, Harwell Campus, Didcot, UK)
B. Malik, P. Fratta, L. Greensmith (Department of Neuromuscular Diseases, UCL Queen Square Institute of Neurology, London, UK)
R. Manzano (Department of Physiology, Anatomy and Genetics, University of Oxford, UK)

G. Sorarú (Department of Neurosciences, Neurology Unit, University of Padova, Italy; Venetian Institute of Molecular Medicine (VIMM), Padova, Italy)
M. Pennuto (Venetian Institute of Molecular Medicine (VIMM), Padova, Italy; Department of Biomedical Sciences, University of Padova, Italy)
M.A. Wood, C. Rinaldi (Department of Paediatrics, University of Oxford, UK; MDUK Oxford Neuromuscular Centre, University of Oxford, UK)

Androgens and androgen-related molecules exert a plethora of functions across different tissues, mainly through binding to the transcription factor androgen receptor (AR). Despite widespread therapeutic use and misuse of androgens as potent anabolic agents, the molecular mechanisms of this effect on skeletal muscle are currently unknown. Muscle mass in adulthood is mainly regulated by the bone morphogenetic protein (BMP) axis of the transforming growth factor (TGF)- β pathway via recruitment of mothers against decapentaplegic homolog 4 (SMAD4) protein. Here we show that, upon activation, AR forms a transcriptional complex with SMAD4 to orchestrate a muscle hypertrophy programme by modulating SMAD4 chromatin binding dynamics and enhancing its transactivation activity.

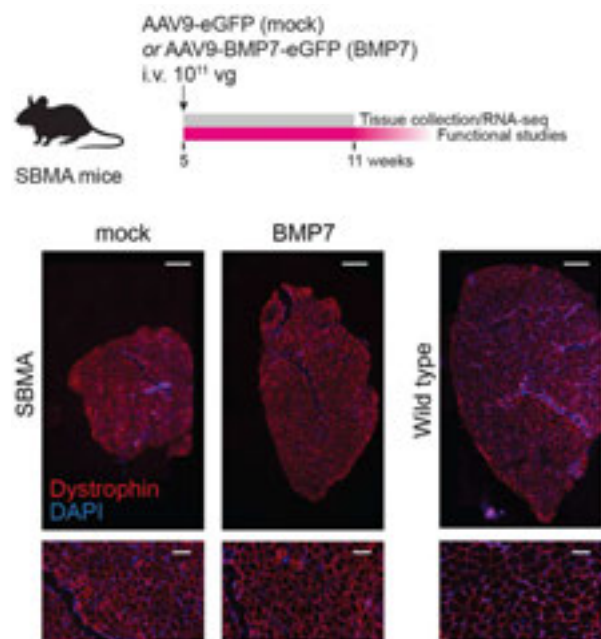
We challenged this mechanism of action using spinal and bulbar muscular atrophy (SBMA) as a model of study. This adult-onset neuromuscular disease is caused by a polyglutamine expansion (polyQ) in AR and is characterized by progressive muscle weakness and atrophy secondary to a combination of lower motor neuron degeneration and primary muscle atrophy. Here we found that the presence of an elongated polyQ tract impairs AR cooperativity with SMAD4, leading to an inability to mount an effective anti-atrophy gene expression programme in skeletal muscle in response to denervation. Furthermore, adeno-associated virus, serotype 9 (AAV9)-mediated muscle-restricted delivery of BMP7 is able to rescue the muscle atrophy in SBMA mice, supporting the development of treatments able to fine-tune AR-SMAD4 transcriptional cooperativity as a promising target for SBMA and other conditions associated with muscle loss.

Reproduced from Forouhan, M., Lim, W.F., Zanetti-Domingues, L.C. et al. AR cooperates with SMAD4 to maintain skeletal muscle homeostasis. *Acta Neuropathol* **143**, 713–731 (2022), under the terms of a Creative Commons Attribution (CC BY) license (<http://creativecommons.org/licenses/by/4.0/>) doi: 10.1007/s00401-022-02428-1

Contact:

C. Rinaldi

carlo.rinaldi@paediatrics.ox.ac.uk



AAV9-mediated delivery of BMP7 in skeletal muscle counteracts muscle atrophy in spinal and bulbar muscular atrophy (SBMA). (Top) Experimental design; arrow indicates the timing of the intravenous (i.v.) injection. Dose is expressed as vector genome (vg). (Bottom) Whole-muscle cross section of TA muscle stained with dystrophin (red) and DAPI (blue) showing partial restoration of muscle atrophy in SBMA muscle upon treatment with BMP7. Scale bar, 1 mm (top) and 100 μ m (below).

Mycosin VI regulates the spatial organisation of mammalian transcription initiation

Y. Hari-Gupta, H.C.W. Reed (School of Biosciences, University of Kent, UK)
N. Fili, Á. dos Santos A.W. Cook, R.E. Gough, C.P. Toseland (Department of Oncology and Metabolism, University of Sheffield, UK)
L. Wang, M. Martin-Fernandez (Central Laser Facility, Research Complex at Harwell, STFC Rutherford Appleton Laboratory, Harwell Campus, Didcot, UK)
J. Aaron, E. Wait, T-L. Chew (Advanced Imaging Center, HHMI Janelia Research Campus, Ashburn, VA, USA)

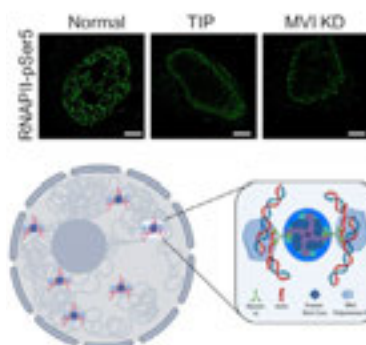
T. Venit (Science Division, Biology Program, New York University Abu Dhabi (NYUAD), Abu Dhabi, United Arab Emirates)
A. Grosse-Berkenbusch, J.C.M. Gebhardt (Institute of Biophysics, Ulm University, Germany)
P. Percipalle (Science Division, Biology Program, New York University Abu Dhabi (NYUAD), Abu Dhabi, United Arab Emirates; Department of Molecular Bioscience, The Wenner Gren Institute, Stockholm University, Sweden)

During transcription, RNA Polymerase II (RNAPII) is spatially organised within the nucleus into clusters that correlate with transcription activity. While this is a hallmark of genome regulation in mammalian cells, the mechanisms concerning the assembly, organisation and stability remain unknown. Here, we have used combination of single molecule imaging and genomic approaches to explore the role of nuclear myosin VI (MVI) in the nanoscale organisation of RNAPII. We reveal that MVI in the nucleus acts as the molecular anchor that holds RNAPII in high density clusters. Perturbation of MVI leads to the disruption of RNAPII localisation, chromatin organisation and subsequently a decrease in gene expression. Overall, we uncover the fundamental role of MVI in the spatial regulation of gene expression.

Reproduced from Hari-Gupta, Y., Fili, N., dos Santos, Á. et al. Myosin VI regulates the spatial organisation of mammalian transcription initiation. *Nat Commun* **13**, 1346 (2022) under the terms of a Creative Commons Attribution (CC BY) license (<http://creativecommons.org/licenses/by/4.0/>). doi:10.1038/s41467-022-28962-w

Contact:

C.P. Toseland
c.toseland@sheffield.ac.uk



Top: Cartoon depiction of the MVI key features including the cargo-binding domain (CBD).

Bottom: Schematic of myosin VI anchoring RNAPII at transcription factories.

In Situ Sol-Gel Synthesis of Unique Silica Structures Using Airborne Assembly: Implications for In-Air Reactive Manufacturing

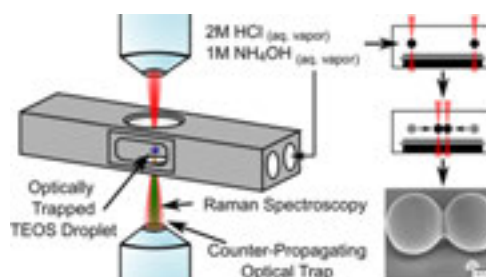
C.R. Barker (Department of Earth Sciences, Royal Holloway University of London, UK; Central Laser Facility, Research Complex at Harwell, STFC Rutherford Appleton Laboratory, Harwell Campus, Didcot, UK)

F.K. Lewns, G. Poologasundarampillai (School of Dentistry, University of Birmingham, UK)
A.D. Ward (Central Laser Facility, Research Complex at Harwell, STFC Rutherford Appleton Laboratory, Harwell Campus, Didcot, UK)

Optical trapping enables the real-time manipulation and observation of morphological evolution of individual particles during reaction chemistry. Here, optical trapping was used in combination with Raman spectroscopy to conduct airborne assembly and kinetic experiments. Micro-droplets of alkoxy silane were levitated in air prior to undergoing either acid- or base-catalyzed sol-gel reaction chemistry to form silica particles. The evolution of the reaction was monitored in real-time; Raman and Mie spectroscopies confirmed the in situ formation of silica particles from alkoxy silane droplets as the product of successive hydrolysis and condensation reactions, with faster reaction kinetics in acid catalysis. Hydrolysis and condensation were accompanied by a reduction in droplet volume and silica formation. Two airborne particles undergoing solidification could be assembled into unique 3D structures such as dumb-bell shapes by manipulating a controlled collision.

Our results provide a pipeline combining spectroscopy with optical microscopy and nanoscale FIB-SEM imaging to enable chemical and structural insights, with the opportunity to apply this methodology to probe structure formation during reactive inkjet printing.

Reproduced from *ACS Appl. Nano Mater.* 2022, **5**, 8, 11699–11706, published by the American Chemical Society, under the terms of a Creative Commons Attribution (CC BY) license (<http://creativecommons.org/licenses/by/4.0/>). doi: 10.1021/acsnm.2c02683



Contact:

G. Poologasundarampillai
g.poologasundarampillai@bham.ac.uk

A.D. Ward
andy.ward@stfc.ac.uk

Correlative multi-scale cryo-imaging unveils SARS-CoV-2 assembly and egress

L. Mendonça, A-S. Krebs, L. Chen, T. Ni (Division of Structural Biology, Wellcome Trust Centre for Human Genetics, University of Oxford, UK)
 P. Zhang (Division of Structural Biology, Wellcome Trust Centre for Human Genetics, University of Oxford, UK; Diamond Light Source, Harwell Science and Innovation Campus, Didcot, UK; Department of Structural Biology, University of Pittsburgh, Pennsylvania, USA)
 A. Howe, J.B. Gilchrist, Y. Sheng, J. Radecke, I. Kounatidis, M.A. Koronfel, M. Harkioliaki (Diamond Light Source, Harwell Science and Innovation Campus, Didcot, UK)

D. Sun (Department of Structural Biology, University of Pittsburgh, Pennsylvania, USA)
 M.L. Knight, W. James (Sir William Dunn School of Pathology, University of Oxford, UK)
 L.C. Zanetti-Domingues, B. Bateman, M. Szykiewicz, M.L. Martin-Fernandez (Central Laser Facility, Research Complex at Harwell, STFC Rutherford Appleton Laboratory, Harwell Campus, Didcot, UK)
 V.D. Li (Murray Edwards College, University of Cambridge, UK)

Since the outbreak of the SARS-CoV-2 pandemic, there have been intense structural studies on purified viral components and inactivated viruses. However, structural and ultrastructural evidence on how the SARS-CoV-2 infection progresses in the native cellular context is scarce, and there is a lack of comprehensive knowledge on the SARS-CoV-2 replicative cycle. To correlate cytopathic events induced by SARS-CoV-2 with virus replication processes in frozen-hydrated cells, we established a unique multi-modal, multi-scale cryo-correlative platform to image SARS-CoV-2 infection in Vero cells.

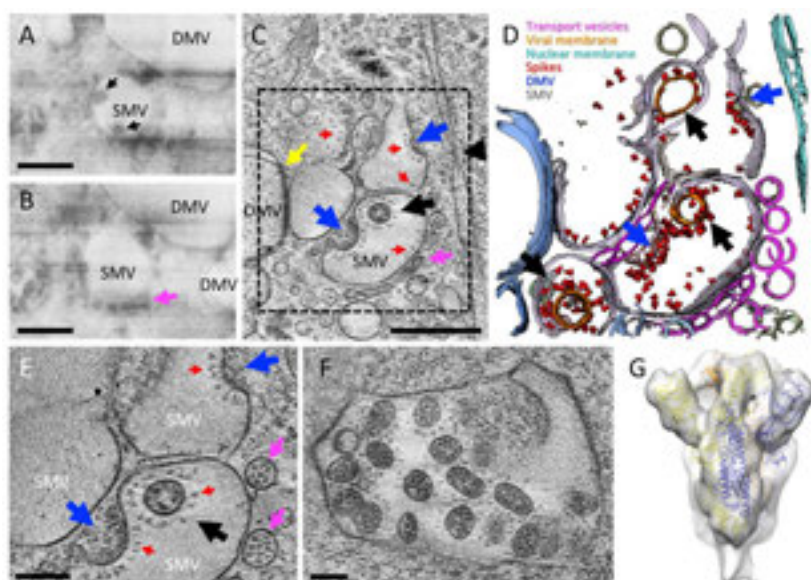
This platform combines serial cryoFIB/ SEM volume imaging and soft X-ray cryo-tomography with cell lamellae-based cryo-electron tomography (cryoET) and subtomogram averaging. Here we report critical SARS-CoV-2 structural events – e.g. viral RNA transport portals, virus assembly intermediates, virus egress pathway, and native virus spike structures, in the context of whole-cell volumes revealing drastic cytopathic changes. This integrated approach allows a holistic view of SARS-CoV-2 infection, from the whole cell to individual molecules.

Reproduced from Mendonça, L., Howe, A., Gilchrist, J.B. et al. Correlative multi-scale cryo-imaging unveils SARS-CoV-2 assembly and egress. *Nat Commun* **12**, 4629 (2021), under the terms of a Creative Commons Attribution (CC BY) license (<http://creativecommons.org/licenses/by/4.0/>). doi: 10.1038/s41467-021-24887-y

Contact:

P. Zhang

peijun.zhang@strubi.ox.ac.uk



SARS-CoV-2 cytoplasmic viral assembly.

(A-B) CryoFIB/SEM images of two sequential slices separated by 80 nm. Black arrows point to virus particles in single membrane vesicle (SMV). Pink arrow points to small dense vesicles lining the outside of virus-containing SMV.
 (C) Tomographic slice of cryoFIB lamella depicting SARS-CoV-2 assembly, with DMV portals (yellow arrow), assembling viruses (blue arrow), assembled virus (black arrow), viral spikes on SMV membranes (red arrows), dense vesicles around the assembly site (pink arrow, as in B) and a nucleopore (black arrowhead).
 (D) Density segmentation of C, displaying three virus particles (black arrows) and two assembly sites (blue arrows).
 (E) An enlarged view (at a different angle) of boxed area in C, showing assembled virus (black arrow), assembling viruses (blue arrows), spikes (red arrows) and spike-containing vesicles (pink arrows).
 (F) Large intracellular virus-containing vesicle (LVCV) full of readily assembled viruses.
 (G) Subtomogram average of viral spikes of intracellular viruses from cell lamellae at 11 Å resolution, fitted with an atomic model of spike trimer (PDB 6ZB5) (Toelzer et al., 2020). Scale bar is 300 nm in A, B and C; and 100 nm in E and F.

Shining Light on Metalloenzyme Catalysis

P.A. Ash, R. Frew (School of Chemistry, University of Leicester, UK; Leicester Institute of Structural & Chemical Biology, University of Leicester, UK)

R.M. Evans, P. Rodríguez Maciá (Department of Chemistry, University of Oxford, Inorganic Chemistry Laboratory, UK)

S.B. Carr (Research Complex at Harwell, STFC Rutherford Appleton Laboratory, Harwell Campus, Didcot, UK)

G. Greetham, I. Sazanovich (Central Laser Facility, Research Complex at Harwell, STFC Rutherford Appleton Laboratory, Harwell Campus, Didcot, UK)

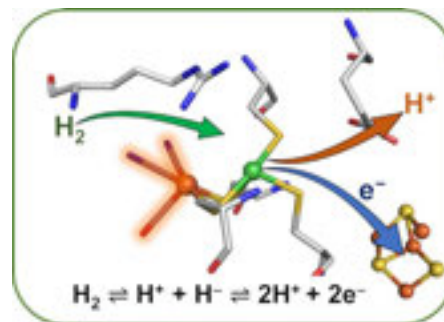
In this study we demonstrate the potential of time-resolved multiple probe spectroscopy (TRMPS) at Ultra to provide unique insight into proton-coupled electron transfer reactions in biology. By exploiting an intrinsically photosensitive step during the [NiFe] hydrogenase catalytic cycle, we are able to track the movement of a proton (H^+) relative to electron transfer on mechanistically-relevant timescales. The TRMPS method is sufficiently sensitive to allow detection of low-intensity transient intermediates in dilute (*ca* mM) biological samples. Here we have established proof-of-concept methodologies that will allow detailed interrogation of biological proton-coupled electron transfer via photodissociation of intrinsic or extrinsic ligands at metalloenzyme active sites. Proton-coupled electron transfer is ubiquitous in nature, and underpins the efficiency of metalloenzymes that catalyse thermodynamically 'difficult' reactions under ambient conditions using earth-abundant metals.

A deep understanding of metalloenzyme mechanisms is needed in order to inspire a new generation of catalysts for sustainable, 'green' energy-conversion processes.

Contact:

P.A. Ash

philip.ash@leicester.ac.uk



Activation of H_2 by [NiFe] hydrogenase enzymes is reliant upon the highly coordinated movement of protons (H^+) and electrons (e^-), and serves as a paradigm for studying biological proton-coupled electron transfer.

A flexible mid-IR laser with high power for temperature-jump spectroscopy

A.E. Edmeades, M. Towrie, P.M. Donaldson (Central Laser Facility, Research Complex at Harwell, STFC Rutherford Appleton Laboratory, Harwell Campus, Didcot, UK)

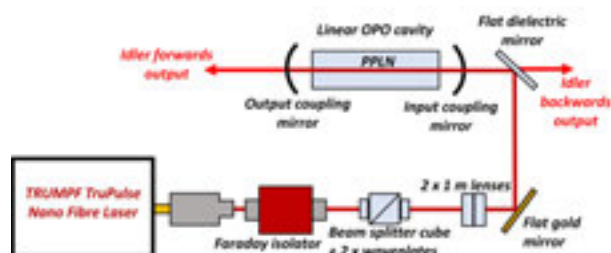
Time resolved temperature-jump (T-jump) infrared (IR) spectroscopy using pulsed laser techniques is a promising method for studying thermally activated processes in catalysis. The current T-jump setup in Ultra-B delivers 70 μ J pulses of 1 ns duration at 1 kHz. Up to 2 mJ of total laser energy can be delivered by using 30 successive laser pulses, achieving higher, more sustained T-jumps. We present a new mid-IR wavelength tunable laser based on a nanosecond pulsed fibre pumping a signal resonant periodically poled lithium niobate (PPLN) optical parametric oscillator (OPO).

Pulse energies of up to 100 μ J at 84 kHz have been observed. This new laser is capable of inducing greater heating on a μ s timescale than the existing 1 kHz system. Flexibility in the fibre laser parameters combined with the IR wavelength tunability provides the opportunity to design pulse sequences to control heating and cooling times for a wide range of samples.

Contact:

A.E. Edmeades

amy.edmeades@stfc.ac.uk



A T-jump laser setup based on a Nd fibre laser and PPLN OPO.

Kerr gated Raman spectroscopy as a diagnostic for high states of electrochemical lithium intercalation into graphite electrodes for Li-ion cells

L. J. Hardwick, A. R. Neale, D. C. Milan, T. Samarakoon F. Braga (Stephenson Institute for Renewable Energy, Department of Chemistry, University of Liverpool, UK)

I. V. Sazanovich (Central Laser Facility, Research Complex at Harwell, STFC Rutherford Appleton Laboratory, Harwell Campus, Didcot, UK)

The general applicability of Kerr gated Raman spectroscopy as a strong diagnostic tool for tracking high states of charge in graphitic electrodes has been expanded through combinations of ex situ and operando spectroelectrochemical experiments.

The approximate sensitivity of the graphitic G-band towards lithiation at high states from $\text{Li}_{0.5}\text{C}_6$ to LiC_6 was found to be a general observation; consistent across different graphite materials and electrolyte formulations (Figure 1), and experimental conditions, and was retained in subsequent cycles (Figure 2).

While this information is often lost underneath emission baselines in conventional Raman investigations of electrochemical intercalation into graphite, these findings further strengthen the potential of Kerr gated Raman spectroscopy as a powerful tool to track the high states of charge in graphite-based electrodes in Li-ion cells.

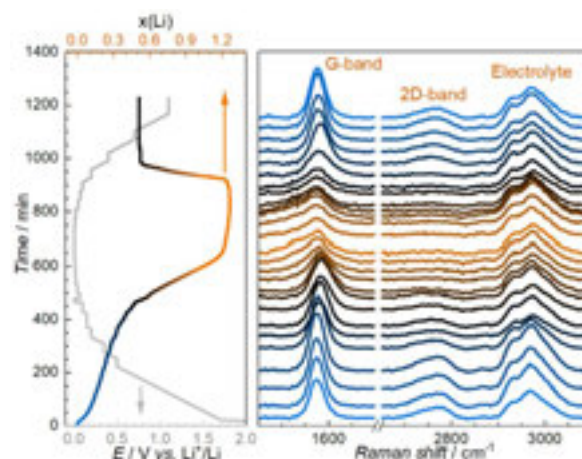


Figure 1: (a) Potential sweep/hold potential and changes in cell capacity (x in Li_xC_6) of the graphite electrode and (b) the operando Kerr gated Raman spectra showing the primary G and 2D graphite bands at 1580 and 2780 cm^{-1} , respectively (electrolyte bands at ca. 2980 cm^{-1}).

Contact:

L. J. Hardwick

hardwick@liverpool.ac.uk

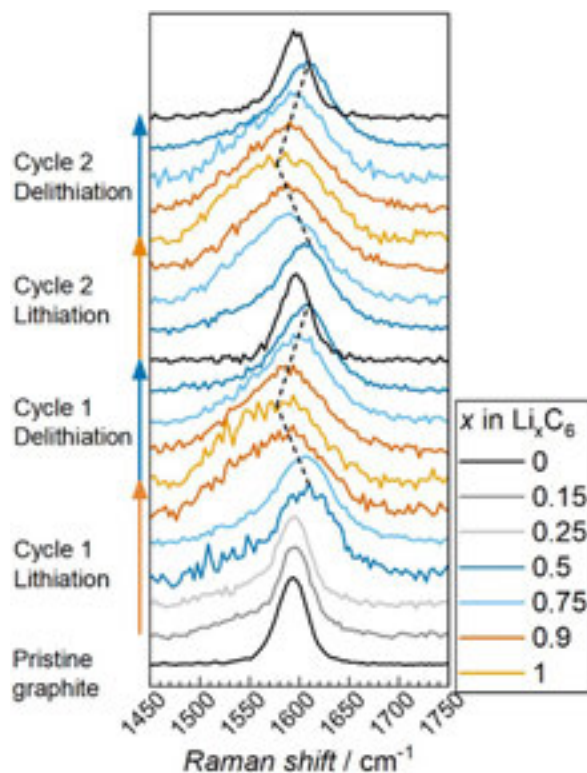


Figure 2: Ex situ Kerr gated Raman spectra (normalised) of SFG-6 graphite electrodes cycled to various states of intercalation (x in Li_xC_6). The dashed lines show an approximation of the band shift for each cycle.

2D-IR Spectroscopy Reveals Structural and Dynamical Details of [NiFe] Hydrogenases

C.C.M. Bernitzky, M. Horch, Y. Rippers (Department of Physics, Freie Universität Berlin, Germany)

G.M. Greetham (Central Laser Facility, Research Complex at Harwell, STFC Rutherford Appleton Laboratory, Harwell Campus, Didcot, UK)

O. Lenz, C. Lorent, J. Schoknecht, C. Schulz, I. Zebger (Department of Chemistry, Technische Universität Berlin, Germany)

N.T. Hunt, A. Parkin, B. Procacci, J. Walton, S.L.D. Wrathall (Department of Chemistry and York Biomedical Research Institute, University of York, UK)

Utilising active-site CO/CN⁻ ligands as vibrational reporter groups (A), we have studied hydrogen-transforming enzymes, so-called hydrogenases, by pump-probe and two-dimensional (2D) infrared (IR) techniques. 2D-IR spectroscopy verified unusual vibrational features of a unique [NiFe] hydrogenase (B) and allowed insights into the constrained structure of its oxygen-protected state (doi:10.1021/jacs.2c06400). Moreover, detailed information on CO bond properties of multiple redox-structural states of the active site were obtained.

The data indicate that the CO bond dissociation energy does not follow the trend of the CO-stretch fundamental frequency (C) but is significantly affected by the shape of the bond potential.

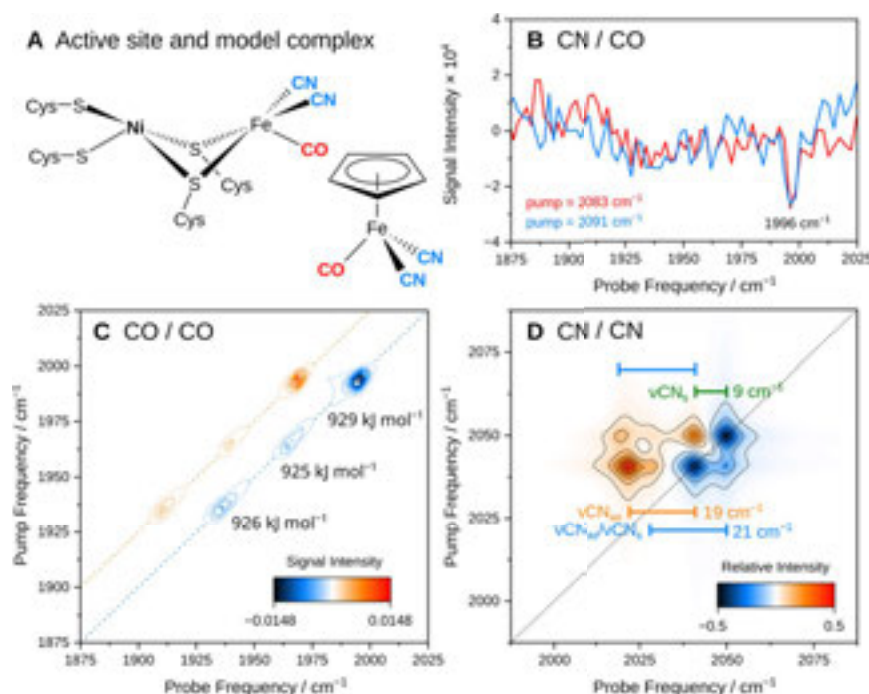
This finding was supported by a study on another hydrogenase (doi:10.1039/D2CP04188J), which additionally revealed differences between the protein-embedded active site and a bioinspired model complex in different solvents (A).

This work also resolved a complex signal pattern related to the CN⁻ ligands, which could be explained and structurally interpreted by quantum chemical calculations (D)(doi:10.3390/catal12090988).

Contact:

M. Horch

marius.horch@fu-berlin.de



(A) Structures of the active site of [NiFe] hydrogenase and a biomimetic model complex. Diatomic ligands used as IR reporter groups are highlighted. (B) Pump slice through the 2D-IR spectrum, revealing coupling between CN stretch modes and a high-frequency CO stretch mode, confirming that the latter reflects an active-site ligand. (C) CO stretch signals of three redox-structural states of the [NiFe] active site, resolved by 2D-IR spectroscopy. Indicated bond dissociation energies do not correlate with CO stretch fundamental frequencies. (D) Simulated 2D-IR spectrum reproducing the experimental CN-stretch signature by including resonant interactions in the underlying calculations.

(B)(C) Reprinted with permission from J. Am. Chem. Soc. 2022, **144**, 37, 17022–17032. Copyright 2022 American Chemical Society. doi: 10.1021/jacs.2c06400
 (A)(D) Reproduced from Catalysts 2022, **12**(9), 988 under the terms and conditions of a Creative Commons Attribution (CC BY) license (<http://creativecommons.org/licenses/by/4.0/>). doi: 10.3390/catal12090988

Temperature-Jump/Drop Infrared Spectroscopy Reveals RNA Tetraloop Refolding Dynamics

C.P. Howe, B. Procacci, N.T. Hunt (Department of Chemistry and York Biomedical Research Institute, University of York, UK)

G.M. Greetham, A.W. Parker (Central Laser Facility, Research Complex at Harwell, STFC Rutherford Appleton Laboratory, Harwell Campus, Didcot, UK)

The structural dynamics of RNA and DNA are essential to cellular function, but direct measurement of folding is challenging. We present a temperature-jump/drop method able to measure both melting and refolding dynamics, and apply it to a series of 12-nucleotide R/DNA sequences featuring the UNCG tetraloop commonly found in biological RNAs.

Stem-loop melting occurred an order of magnitude slower in RNA than DNA, while the refolding dynamics of both sequences required similar timescales. Both melting and refolding followed Arrhenius behaviour, though refolding was characterised by a negative activation energy, consistent with the complex energy landscape of folding initiation.

Placing a single AU pair at key points in the stem showed that RNA sequences begin melting from the loop while DNA hairpins begin melting from the terminal end of the stem. We thus conclude that conformational changes of analogous pairs of RNA and DNA tetraloops proceed by different mechanisms.

References:

J. Phys. Chem. Lett. 2022, 13, 39, 9171–9176

<https://doi.org/10.1021/acs.jpcclett.2c02338>

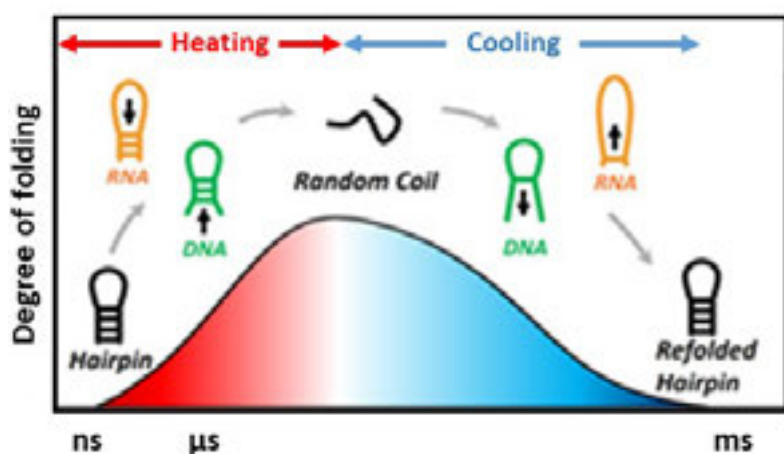
J. Phys. Chem. B 2023, 127, 7, 1586–1597

<https://doi.org/10.1021/acs.jpcc.2c08709>

Contact:

N.T. Hunt

neil.hunt@york.ac.uk



Schematic diagram of the T jump/drop experiment. A ns-duration laser-induced rise in temperature causes hairpin melting followed by fast sample cooling which enables measurement of refolding dynamics.

A comprehensive understanding of carbon–carbon bond formation by alkyne migratory insertion into manganese cycles

L.A. Hammarback, J.B. Eastwood, T.J. Burden, C.J. Pearce, I.J.S. Fairlamb, J.M. Lynam (Department of Chemistry, University of York, UK)

I.P. Clark, M. Towrie (Central Laser Facility, Research Complex at Harwell, STFC Rutherford Appleton Laboratory, Harwell Campus, Didcot, UK)
A. Robinson (Syngenta Crop Protection AG, Munchwilten, Switzerland)

Migratory insertion (MI) is one of the most important processes underpinning the transition metal-catalysed formation of C–C and C–X bonds. In this work, a comprehensive model of MI is presented, based on the direct observation of the states involved in the coupling of alkynes with cyclometallated ligands, augmented with insight from computational chemistry.

Time-resolved spectroscopy demonstrates that photolysis of complexes $[\text{Mn}(\text{C}^{\wedge}\text{N})(\text{CO})_4]$ ($\text{C}^{\wedge}\text{N}$ = cyclometallated ligand) results in ultra-fast dissociation of a CO ligand. Performing the experiment in a toluene solution of an alkyne results in the initial formation of a solvent complex $\text{fac-}[\text{Mn}(\text{C}^{\wedge}\text{N})(\text{toluene})(\text{CO})_3]$. Solvent substitution gives an η^2 -alkyne complex $\text{fac-}[\text{Mn}(\text{C}^{\wedge}\text{N})(\eta^2\text{-R}^1\text{C}_2\text{R}^2)(\text{CO})_3]$ which undergoes MI of the unsaturated ligand into the Mn–C bond. These data allowed for the dependence of second order rate constants for solvent substitution and first order rate constants for C–C bond formation to be determined.

A systematic investigation into the influence of the alkyne and $\text{C}^{\wedge}\text{N}$ ligand on this process is reported.

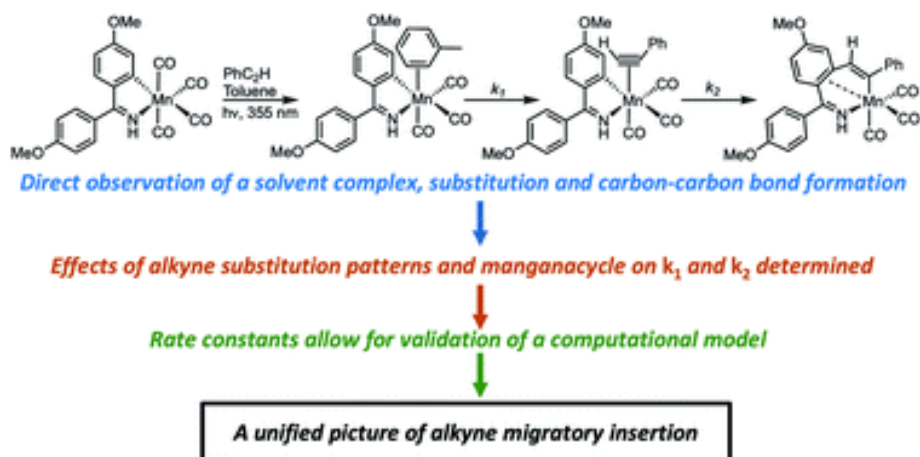
The experimental data enabled the development of a computational model for the MI reaction which demonstrated that a synergic interaction between the metal and the nascent C–C bond controls both the rate and regiochemical outcome of the reaction. The time-resolved spectroscopic method enabled the observation of a multistep reaction occurring over 8 orders of magnitude in time, including the formation of solvent complexes, ligand substitution and two sequential C–C bond formation steps.

Reproduced from L A Hammarback et al Chem. Sci., 2022, 13, 9902-9913, under the terms and conditions of a Creative Commons Attribution (CC BY) license (<http://creativecommons.org/licenses/by/3.0/>).

Contact:

I.J.S. Fairlamb
ian.fairlamb@york.ac.uk

J.M. Lynam
jason.lynam@york.ac.uk



The Influence of the Epigenetic Base 5-methyl-cytosine on DNA Excited State Dynamics

M. Stitch, S.J. Quinn (School of Chemistry, University College Dublin, Ireland)

M. Towrie, A.W. Parker (Central Laser Facility, Research Complex at Harwell, STFC Rutherford Appleton Laboratory, Harwell Campus, Didcot, UK)

The photochemistry of DNA has been exhaustively studied due to its importance in skin cancer, the most common form of cancer (40% of cases globally). However, photochemical studies on sequences containing epigenetic bases¹ have yet to be fully explored. This is remarkable as, for example, modified cytosine in the form of methylated-cytosine (5mC) may be called the fifth base of human DNA, constituting approximately 1% of the bases in mammalian genomes. We apply ultrafast time-resolved infrared spectroscopy to investigate photochemical differences between cytosine and its epigenetic form 5-methyl cytosine, as well as within a model DNA duplex sequence. We identify both similarities and subtle differences between the two bases in terms of their photochemistry.

¹ Bases that have slightly different chemical structure but remain biologically competent and able to perturb cell function, for example leading to the onset of cancer.

Contact:

A.W. Parker

tony.parker@stfc.ac.uk

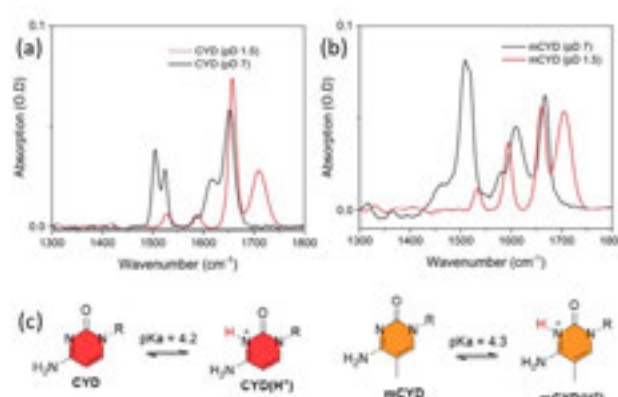


Figure 1: FTIR absorbance spectra of (a) cytidine, (b) 5-methyl-cytidine (mCYD) recorded in D_2O buffer, (c) structures of epigenetic derivatives and reported pK_a values.

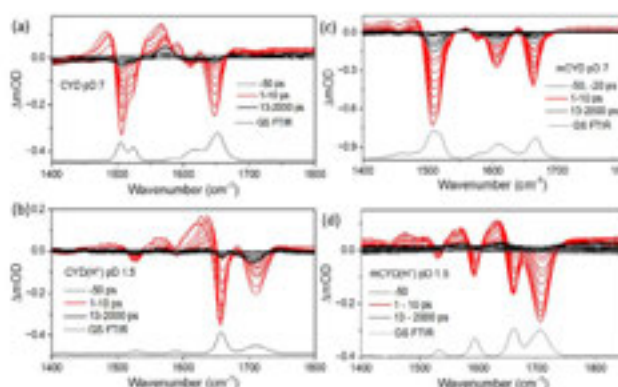


Figure 2: TRIR difference spectra of 10 mM of CYD (a) and (b) and mCYD (c) & (d) in 100 mM K phosphate in D_2O at pH 7 and pH 1.5 ($\lambda_{ex} = 265$ nm, 2 kHz, 150 fs). Removal of 2000 ps delay subtracted, to remove baseline drift associated with hot D_2O .

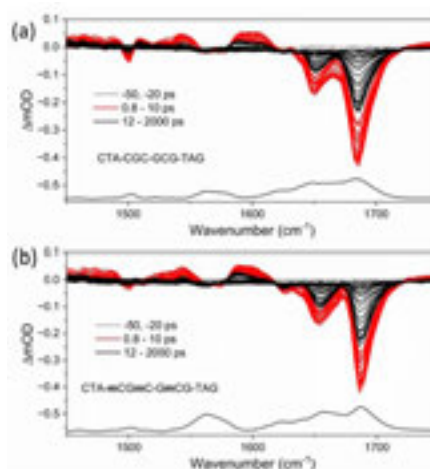


Figure 3: TRIR difference spectra of 10 mM of (a) CTACGCGCGTAG and (b) CTAmCGmCGmCGTAG in 50 mM K phosphate, pH 7, in D_2O ($\lambda_{ex} = 285$ nm, 2 kHz, 150 fs).

G-Quadruplex Binding of an enantiomeric Osmium Polypyridyl Probe Revealed by Time-Resolved Infrared and NMR Solution Studies

M. Stitch, S.J. Quinn (School of Chemistry, University College Dublin, Ireland)
M. Towrie (Central Laser Facility, Research Complex at Harwell, STFC Rutherford Appleton Laboratory, Harwell Campus, Didcot, UK)

K. Peterková, P. Podbevšek, J. Plavec (Slovenian NMR Center, National Institute of Chemistry, Ljubljana, Slovenia)
R.Z. Boota, P.A. Scattergood, P.I.P. Elliott (Department of Chemical Sciences, University of Huddersfield, UK)

Quadruplex DNA structures are important diagnostic and therapeutic targets due to their role in gene regulation, epigenetic processes and their overexpression in oncogenes. These structures adopt various folded topologies that present multiple binding sites. This study reports on the ability of time-resolved infrared spectroscopy (TRIR) to provide information on the binding environment of a NIR emitting polypyridyl osmium complex when bound to two biologically relevant quadruplex structures, human telomere (hTel) and cMYC form.

Visible excitation of the probe reveals the identity of nucleobases in the binding site. In the case of the cMYC structure binding is exclusively through stacking to guanines whose bleach carbonyl bands appear in the TRIR, while in the case of the hTel form the contributions of the thymine and adenine bleaches indicate additional loop interactions. These results are supported by complementary NMR studies and indicates the role that TRIR can play in developing new DNA probes.

Contact:

S.J. Quinn
susan.quinn@ucd.ie

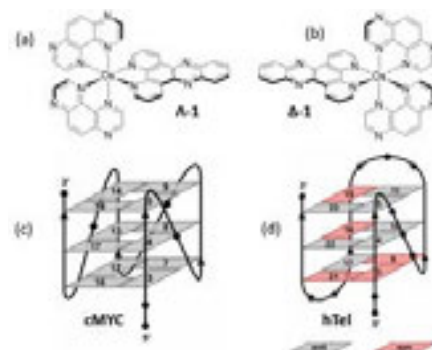


Figure 1: Molecular structures of probe **1** and schematic representation of (a) **cMYC** and (b) **hTel G4** structures.

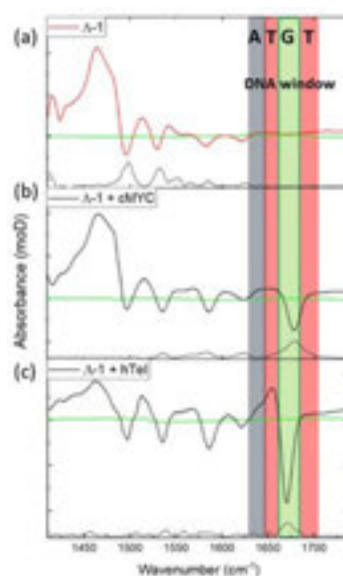


Figure 2: TRIR difference spectra recorded at 50 ps of (a) 0.4 mM of **1** and (b) in the presence of 0.4 mM of **cMYC**, (c) in the presence of 0.4 mM of **hTel** in 25 mM K phosphate and 70 mM KCl, pH 7, 50 ps after $I_{ex} = 400$ nm, 2 kHz, 150 fs).

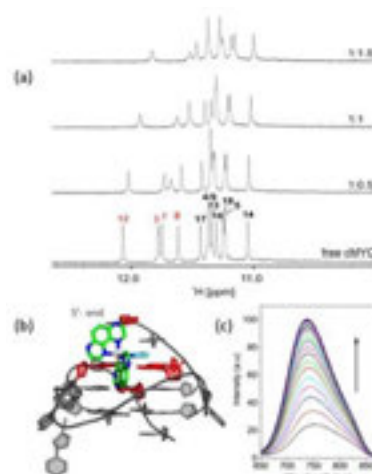


Figure 3: (a) ^1H NMR spectra of the **cMYC**, with increasing $[\Lambda\text{-1}]$ molar equivalents with 70 mM KCl, 25 mM K-phosphate buffer, pH 7, 298 K, in 90% H_2O and 10% D_2O . (b) Modelling of $\Lambda\text{-1}$ with the **cMYC** structure (PDB ID: 2LBV), nucleotides interaction highlighted in red. (c) Change in the emission of $\Lambda\text{-1}$ in the presence of increasing $[\text{cMYC}]$.